Annals of Nuclear Medicine Vol. 16, No. 1, 11–18, 2002

Performance evaluation of OSEM reconstruction algorithm incorporating three-dimensional distance-dependent resolution compensation for brain SPECT: A simulation study

Takashi YOKOI,* Hiroyuki SHINOHARA** and Hideo ONISHI***

**Department of Research and Development for Nuclear Medicine, Shimadzu Corporation*
***Department of Radiological Sciences, Tokyo Metropolitan University of Health Sciences*
****Department of Radiological Sciences, Hiroshima Prefectural College of Health Sciences*

Iterative reconstruction techniques such as an ordered subsets-expectation maximization (OSEM) algorithm can easily incorporated various physical models of attenuation or scatter. We implemented OSEM reconstruction algorithm incorporating compensation for distance-dependent blurring due to the collimator in SPECT. The algorithm was examined by computer simulation to estimate the accuracy for brain perfusion study. ***Methods:*** The detector response was assumed to be a two-dimensional Gauss function and the width of the function varied linearly with the source-to-detector distance. The attenuation compensation (AC) was also included. To investigate the properties of the algorithm, we performed computer simulations with the point source and digital brain phantoms. In the point source phantom, the uniformity of FWHM for the radial, tangential and longitudinal directions was evaluated on the reconstruction image. As for the brain phantom, quantitative accuracy was estimated by comparing the reconstructed images with the true image by the mean square error (MSE) and the ratio of gray and white matter counts (G/W). Both noise free and noisy simulations were examined. ***Results:*** In the point source simulation, FWHM in radial, tangential and longitudinal directions were 14.7, 14.7 and 15.0 mm at the image center and were 15.9, 9.83 and 10.6 mm at a distance of 15 cm from the center by using FBP, respectively. On the other hand, they were 8.12, 8.12 and 7.83 mm at the image center, and were 7.45, 7.44 and 7.01 mm at 15 cm from the center by OSEM with distance-dependent resolution compensation (DRC). An isotropic and stationary resolution was obtained at any location by OSEM with DRC. The spatial resolution was also improved about 6.5 mm by OSEM with DRC at the image center. In the brain phantom simulation, the blurring at the edge of the brain structure was eliminated by using OSEM with both DRC and AC. The G/W was 2.95 and 2.68 for noise free and noisy cases, respectively, when no compensation was performed. But the values for G/W without and with noise became 3.45 and 3.21 with AC only and were improved to 3.75 and 3.71 with both AC and DRC. The G/W approached the true value (4.00) by using OSEM with both AC and DRC even when there was statistical noise. ***Conclusion:*** In conclusion, OSEM reconstruction including the distance-dependent resolution compensation algorithm was reasonably successful in achieving isotropic and stationary resolution and improving the quantitative accuracy for brain perfusion SPECT.

Key words: single photon emission computed tomography (SPECT), distance-dependent blurring, collimator, ordered subset-expectation maximization (OSEM), resolution compensation

Received August 1, 2001, revision accepted September 21, 2001.

For reprint contact: Hiroyuki Shinohara, Ph.D., Department of Radiological Science, Tokyo Metropolitan University of Health Sciences, 2–10 Higashi-ogu 7-chome, Arakawa-ku, Tokyo 116–8511, JAPAN.

E-mail: sinohara@post.metro-hs.ac.jp

INTRODUCTION

THE GAMMA CAMERA makes imaging possible by limiting the direction of the incidence of the γ-ray with the collimator on the detector front. The low spatial resolution of the SPECT image is mainly due to the limited collimator

resolution. This is because the collimator hole diameter must be relatively large to obtain reasonable efficiency, and degradation of the spatial resolution is introduced by oblique entrance of the γ-ray into the detector. So that the spatial resolution, and not only the degradation of resolution, differs at the location of the reconstructed image. Therefore, restoration filters, such as the Wiener filter provide incomplete results due to the anisotropic and non-stationary nature of SPECT reconstruction.

To compensate for source-to-detector distance blurring in SPECT, several methods have been proposed. For example, by using the frequency-distance relationship (FDR), the signal at a distance from the center of rotation is concentrated along lines on the two-dimensional Fourier transform of the sinogram.[1] Therefore an inverse filter which is the reciprocal of the modulation transfer function (MTF) can be applied for an individual signal corresponding to distance in the Fourier domain.[1–7] Ogawa and Katsu[8] proposed another approach removing the oblique component of the γ-ray to the detector due to the geometrical shape of the collimator by iterative processing. Such algorithms are the pre-processing method for the projection data and the corrected projection data are then reconstructed with the usual filtered backprojection (FBP) or ordered subset-expectation maximization (OSEM) algorithm.[9,10] There is the advantage of comparatively fast calculation.

On the other hand, an iterative method such as the OSEM algorithm can easily incorporate various physical models of attenuation[11,12] or scatter.[33,34] Iterative SPECT reconstruction algorithm modeling the distance-dependent detector response can be applied to the emission data to obtain isotropic and stationary estimates of the activity distribution.[13–21] Maniawski et al.[38] demonstrated that varying the distance from the source of activity to the detector provided significant artifacts on Tl-201 cardiac SPECT images due to varying spatial resolution. Although there are many reports about OSEM with distance-dependent resolution compensation (DRC) applied to cardiac SPECT study,[17,24] it is not well known whether DRC is available or not in the brain SPECT study. In this report we evaluated the basic properties of OSEM with DRC by computer simulation, and the algorithm was applied the digital brain phantom to estimate accuracy for brain perfusion studies.

THEORY

The basic equation

The basic equation for maximum likelihood-expectation maximization (MLEM) is:

$$\lambda_j^{k+1} = \frac{\lambda_j^k}{\sum_i^n C_{ij}} \sum_i^n \left(\frac{C_{ij} y_i}{\sum_{j'}^m C_{ij} \lambda_{j'}^k} \right), \qquad (1)$$

where λ_j^k is the value of the reconstructed image at pixel j for the k-th iteration, y_i is the measured projection at the i-th bin, and C_{ij} is the detection probability that gives the fraction of photons from pixel j to projection bin i. In the OSEM, it computes all with only the projection data in the subset instead of using all the data simultaneously. In this case, k indicates the updating number of the image.

If there is no blurring at all, this is equivalent to reaching a detector as the narrow-beam γ-ray which is emitted from pixel j. In the conventional OSEM algorithm, the response function of the detector is assumed to be the rectangular form for reconstruction as shown in Figure 1 (a). Of course conventional FBP is used in the same manner for reconstruction. On the other hand, the response function spread to the neighboring pixels and slices which take into account degradation of the resolution are shown in Figure 2 (b). This function agrees with the point spread function (PSF) which is the count distribution by measuring a point source.

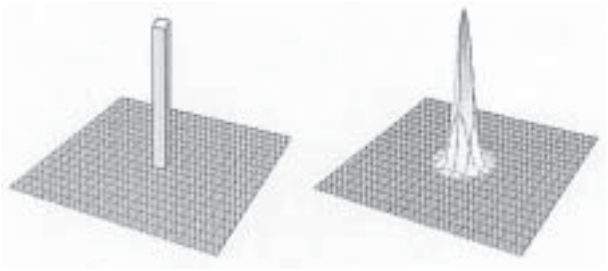

(a) (b)

Fig. 1 The shape of detector response. a) Ideal detector response. b) Blurring detector response which corresponds the photon count density distribution at the detector surface when a point source is imaged using a gamma camera (point spread function).

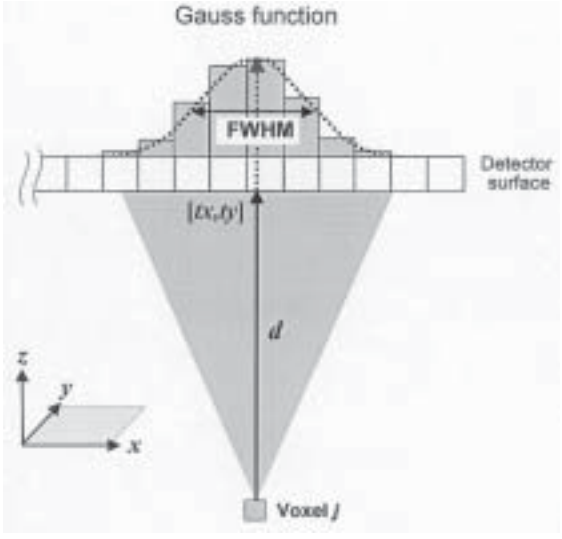

Fig. 2 The detector response was assumed to a 2D Gauss function. The width of Gauss function varied with the distance from γ-ray source to detector surface.

Definition of the response function depend on distance
First of all, the following three assumptions[22,23] are introduced to formulate the response function: 1) the blurring of the detector can be defined by the Gauss function; 2) the full width at half maximum (FWHM) of the response function varied linearly with the distance between the detector and source; and 3) FWHM of the *x* (horizontal) and *y* (vertical) directions of the detector are the same as each other. There is the following simple relationship between FWHM and distance *d*:

$$\text{FWHM} = a \times d + b, \qquad (2)$$

where *a* and *b* are constant and are precalculated by linear regression analysis measuring at various *d* with the point source. Now, defining the coordinate system as shown in Figure 2, a two-dimensional Gauss function is generated around the γ-ray incidence point [*tx*, *ty*] with the next equation:

$$h(x,y,d) = \frac{1}{2\pi\sigma^2(d)}\, e^{-\frac{r^2}{2\sigma^2(d)}}, \qquad (3)$$

where $\sigma(d)$ is the standard deviation as a function of distance *d*, and *r* is the distance from the pixel [*x*, *y*] to [*tx*, *ty*] as follows:

$$r = \sqrt{(x - tx)^2 + (y - ty)^2}. \qquad (4)$$

The relationship between $\sigma(d)$ and FWHM is expressed as,

$$\sigma(d) = \sqrt{\frac{1}{8 \ln 2}}\ \text{FWHM} \cong 0.425\ \text{FWHM}. \qquad (5)$$

Therefore FWHM can be calculated by means of equation (2) if distance *d* is determined, and consequently the response function $h(x,y,d)$ can be calculated by substituting equations (4) and (5) into equation (3). This function should be interpreted as being the response of the whole detector system including the collimator.

Inclusion detector response and attenuation into detection probability
Detection probability C_{ij} can be defined as the fraction of photons emitted from voxel *j* in the reconstruction space to reaching detector *i*. Therefore $h(x,y,d)$ in equation (3) indicates the detection probability itself. Because the probability is spread out in the slice direction (*y*), we conveniently used the notation $C_{[x,y]j}$ as detection probability in equation (1). If total probability of observing a photon is assumed to be unity measured at a certain projection angle, detection probability was then redefined by performing the following normalization:

$$C_{[x,y]j} = \frac{h(x,y,d)}{\sum_r h(x,y,d)}. \qquad (6)$$

Attenuation compensation (AC) was also included in the present algorithm. The attenuation factor is given by $\exp\left(-\sum_{j\in J_i} \mu_j l_{ij}\right)$, where μ_j is the linear attenuation coefficient [cm^{-1}] at voxel *j*, J_i is the subset of pixels passing through the *i*-th ray and l_{ij} is the intersection length [cm]. The μ-map is supplied as a prior information measured by the external source or X-ray CT scanner. The μ-map is assumed to vary slowly within the acceptance angle of collimator holes, so the attenuation factor was calculated approximately only along the central path from each voxel.[16,24] The probability of incorporating the attenuation consists in calculating $C_{[x,y]j}\exp\left(-\sum_{j\in J_i} \mu_j l_{ij}\right)$.

Projector and backprojector
In the OSEM algorithm, the reconstruction image can be obtained by repeating the projector-backprojector pair. The forward projection involving 3D resolution compensation computes the weighted linear summation by using detector probability $C_{[x,y]j}$ as the convolution kernel. Backprojection becomes the inverse of forward projection. This convolution operation in the projector/backprojector provides weighted smoothing. When incorporating resolution compensation, the computation of this process is added and this increases calculation time.

METHODS

Computer simulations
To evaluate the performance of the present algorithm, we carried out the computer simulations with the point source and digital brain phantoms. The size of the phantoms was 128 × 128 × 128 cubic pixel with a pixel size of 0.3125 cm. In the point source phantom, the spheres with a five-pixel diameter were placed 0, ±5.0, ±10.0 and ±15.0 cm from the image center on the central slice, and no attenuating medium was assumed. This phantom was used to investigate the basic properties of the algorithm and to test the implemented program.

In the brain phantom, the activity distribution map was modeled by the gray and white matter structures segmented from the autopsy brain phantom.[25,26] The activity ratio of gray/white matter was assumed to be 4 : 1. The same image was used in all the slices. An attenuation map was made by scaling the outline of the activity distribution, and filled with the constant linear attenuation coefficient μ in the tissue and skull regions. To simulate a Tc-99m study, the μ values for the narrow beam of 141 keV were assumed to be 0.15 and 0.26 cm^{-1} for tissue and skull, respectively.

The simulated collimator was a low-energy high-resolution (LEHR) parallel-hole collimator for Tc-99m on a triple-head gamma camera (PRISM-3000XP, Marconi) as previously reported by Pan et al.[19]

$$\text{FWHM [cm]} = 0.0513d - 0.119. \qquad (7)$$

The simulation data were generated from the each phantom by convoluting a Gauss function (σ = ±2.0). Furthermore, the projection data were also attenuated along the corresponding attenuation path in the brain

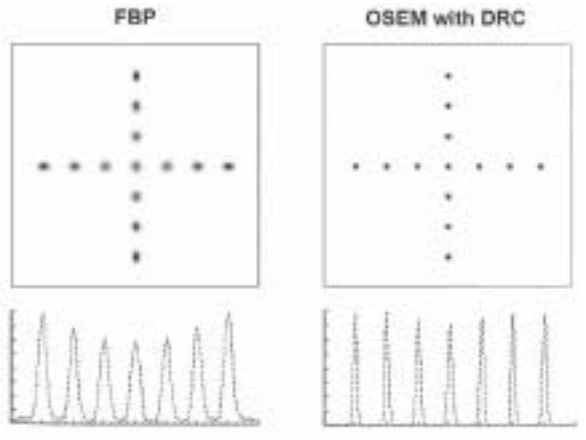

Fig. 3 Reconstructed images of the central slice in the 3D point source phantom by using a) FBP and b) OSEM with DRC (subset = 2, iteration number = 25). The simulated projection data included the effect of detector response only. Profiles through the horizontal line for the reconstructed images by each method. The spatial resolution by OSEM with DRC was significantly improved than that using FBP.

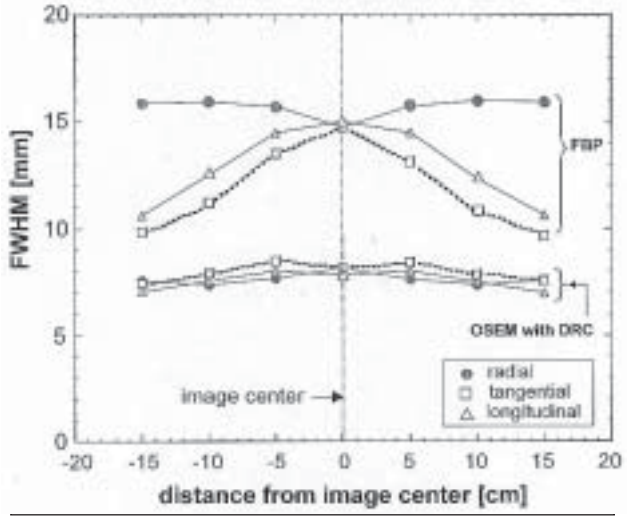

Fig. 4 Estimated FWHM at each location of the point sources in the radial (●), tangential (□) and longitudinal (△) directions calculated by a) FBP and b) OSEM (subset = 2, iteration number = 25) with DRC. An isotopic and stationary spatial resolution was obtained using OSEM with DRC at every location.

phantom simulation. Each projection data set consisted of 120 angles with a 128 × 128 matrix, and a 25 cm radius circular orbit was assumed. Poisson statistical noise[36] was added to the generated projection data from the brain phantom. In all simulations no Compton scatter effect was involved at all since we were interested in examining how distance-dependent resolution compensation would work effectively. The program was implemented using Visual C++6.0 (Microsoft Inc.) and a personal computer (Pentium-III, 600 MHz, 192 MB memory).

Evaluation

To investigate the performance and basic properties of the DRC algorithm, the uniformity of FWHM for the radial, tangential and longitudinal directions was evaluated for each point source on the reconstructed image. The iteration number was varied from 1 to 30 with a subset size of 2. The reconstruction was performed by OSEM with DRC only because the point source phantom was assumed to be attenuation free. For comparison, the reconstruction was also performed by FBP with no compensation. In addition, the ideal projection data by means of which the same point source was reprojected with a narrow-beam were reconstructed by using the usual OSEM algorithm without any compensation. The iteration number was 30 with a subset of 2. The probability of C_{ij} was calculated as the area of overlap between the line from detector i and pixel j, and details of this algorithm were previously reported.[37] The reprojection for generation of the ideal data was performed with the same C_{ij} and projector algorithm. As a result, because it converged on 8.01 mm FWHM, this value was employed as the ideal FWHM.

As for the brain phantom study, the quantitative accuracy was estimated by comparing the reconstructed images with the true image by using the mean squares error (MSE) and the ratio of gray to white matter counts (G/W). Three reconstruction strategies with OSEM were performed with: a) no compensation, b) AC only and c) both AC and DRC simultaneously. Both noise free and noisy simulations were examined. The subset size used was 8. The rectangular (3 × 3 pixels) regions of interest (ROI) were defined at the gray matter (superior temporal gyrus) and white matter (corpus callosum).

RESULTS AND DISCUSSION

Point source simulation

Figure 3 shows the images reconstructed by means of FBP and OSEM with DRC at the iteration number 25 and subset size 2. The reconstructed image demonstrates improvements in uniformity and sharpening of each point source by OSEM with DRC. The profile curves through the horizontal line for each image were also indicated. In the FBP method, the peak intensity declined in the region of the image center, and an entire broad profile curve was found. The relative intensity in the central region was decreased by approximately 25% compared with the edge region. The reason for the decline in the peak in the central region seems to be that the response function was spread out due to the resolution degradation, but not the attenuation because each point source was set in the air. On the other hand, the peak intensity was recovered in the central region by the OSEM with DRC.

In Figure 4 are plotted the FWHM in radial, tangential and longitudinal directions at each point source for these reconstructed images. In the FBP method, the estimated FWHM were 14.7, 14.7 and 15.0 mm in radial, tangential

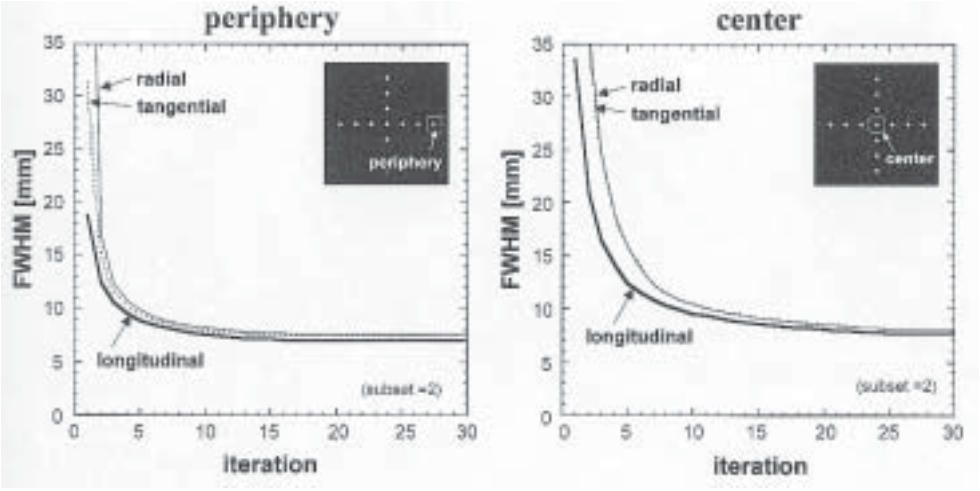

Fig. 5 FWHM in radial, tangential and longitudinal directions versus iterative number. FWHM were determined from the point source phantom by using OSEM reconstruction with DRC. The notations of "periphery" and "center" represent the location of point source at 15 cm and 0 cm from the image center, respectively.

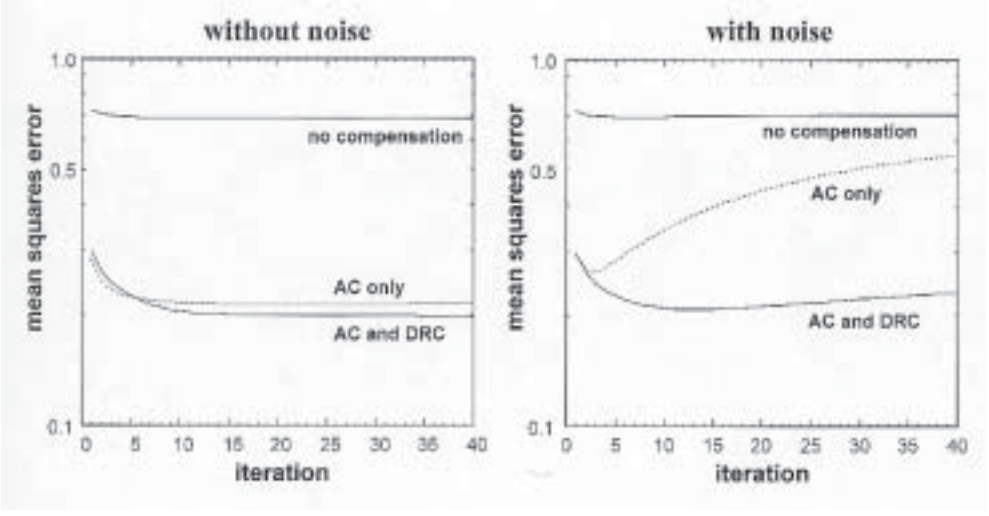

Fig. 6 Mean squares error (MSE) difference between the reconstructed images and true phantom image is plotted as a function of the iteration number for noise free and noisy simulations. The OSEM reconstruction includes no compensation, attenuation compensation (AC) only and both AC and DRC. Subset size was 8.

and longitudinal directions at the image center, so that the spatial resolution was almost isotropic. Nevertheless anisotropic FWHM was found to leave the center and became 15.9, 9.83 and 10.6 mm in the radial, tangential and longitudinal directions, respectively. On the other hand, the FWHM in those using OSEM with DRC were 8.12, 8.12 and 7.83 mm at the image center and were 7.45, 7.44 and 7.01 mm at the periphery. An isotropic and stationary resolution was obtained at any location by OSEM with DRC. Resolution almost recovered the ideal value (8.01 mm), and the 6.5-mm improvement (from 14.7 mm to 8.12 mm at the center) was obtained with the DRC algorithm. The degree of improvement was almost completely consistent with the results reported by Formiconi et al.[14] (from 15 mm to 9 mm), but a tendency towards small over-correction was observed with DRC in the periphery region for the point source. A reasonable explanation for over-correction seemed to be the roughness of the sampling point when generating a Gauss function. The Gauss function was approximated in the rectangle form shown in Figure 2, so there was an error due to rapid change in Gauss function near the collimator. When doing more precise resolution correction, a finer sampling acquisition would be needed. Because this introduces an increase in total computing time, it is impossible to do finer sampling with present computer performance, but this seemed to have little effect on quantitation in a routine study because the error was equal to or less than 1 mm.

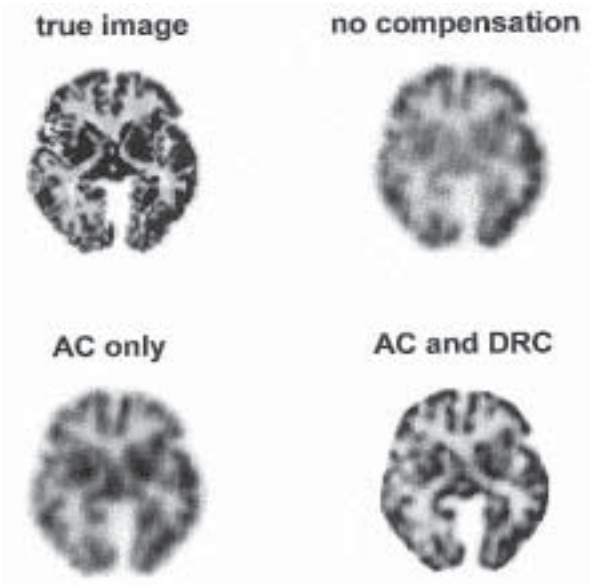

Fig. 7 Brain phantom results without statistical noise. The reconstruction includes no compensation (iteration number = 5), attenuation compensation (AC) only (iteration number = 5) and both AC and DRC (iteration number = 30) with a subset size 8. The true image was the original digital phantom. Simulated projection data included the effect of attenuation and detector response. Scatter component was excluded in the simulated projection data. The reconstructed image with both AC and DRC was approached to the true image.

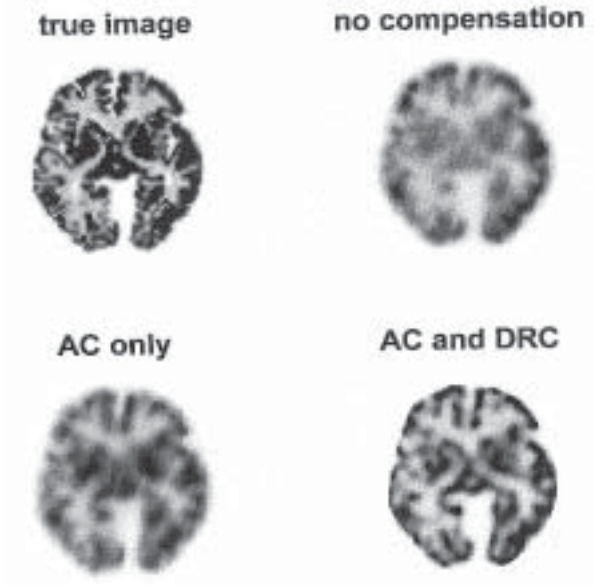

Fig. 8 Brain phantom results with statistical noise. Reconstruction includes no compensation (iteration number = 5), attenuation compensation (AC) only (iteration number = 5) and both AC and DRC (iteration number = 20) with a subset size 8. No prefilter was applied before any reconstruction process. It should be noted that the effect of statistical noise was suppressed with DRC.

Figure 5 shows FWHM measured from the point source by OSEM with DRC at the center and 15 cm from the center for radial, tangential and longitudinal directions as function of the iteration number. The number of iterations needed to reach a constant FWHM was about 20 for the periphery and 25 for the center. The convergence rate was more rapid at the periphery and slower in the center. These results agree with the results reported by Pan et al.[19] and Kohli et al.[21] Kohli et al. concluded that the reason for slow convergency in the central region was the effect of attenuation, but our simulation was assumed to have a no attenuating medium in case of the point source phantom, so the slow convergency cannot be attributed to the attenuation. A reasonable explanation for the slow convergency is that the SPECT resolution is originally better at the periphery than at the center. This seems to be the reason for the rapid convergence rate at the periphery.

Brain phantom simulation

Figure 6 shows the MSE value difference between the reconstructed images and the true phantom image is plotted as function of the iteration number with and without noise. In the noise free case, the usual OSEM required only about 5 iterations to reach a constant MSE. A minimum MSE was achieved for the OSEM results with both AC and DRC, but the MSE was not completely constant even after 35 iterations. On the other hand, a rather different tendency was observed in MSE with noise simulation. With noise, the MSE value with AC decreased rapidly as a function of the iteration number and reached to its minimum point at 4 iterations. Subsequently it increased gradually at late iterations. On applying DRC, the minimum MSE was observed at 13 iterations, and it increased slightly. However, MSE was almost constant and there seemed to be little effect of noise.

Figure 7 is the reconstructed image of the digital brain phantom when using OSEM without any compensation (5 iteration), with AC only (5 iteration) and with both AC and DRC (30 iteration), respectively, in noise free simulation. The true phantom image is also shown for comparison. There was blurring of the surrounding activity into the edge region on the reconstructed images obtained by OSEM without any compensation and with AC only. The structures in the brain were not completely resolved by performing AC alone. We found that the blurring at the edge of the brain structure disappeared on applying the DRC, and the reconstructed image qualitatively approached the true image.

Figure 8 shows the reconstructed images with noise. The iteration numbers were 5, 5 and 20 for no compensation, with AC and with both AC and DRC, respectively. No prefilter was applied before any reconstruction process. It should be noted that the influence of statistical noise was suppressed with DRC. It was likely that Gaussian

convolution kernel to compensate for the distance-dependent detector response behaved as a kind of smoothing filter. Use of the DRC algorithm is expected to improve the spatial resolution without increasing noise in a clinical SPECT study.

The G/W was 2.95 and 2.68 for noise free and noisy cases, respectively, when no compensation was performed. But the G/W values without and with noise became to 3.45 and 3.21 with AC only and those were improved to 3.75 and 3.71 with both AC and DRC. Combining the DRC with AC approached the true value (4.00) compared with AC only because DRC reduced the effect of partial volume. It can be concluded that full recovery was not achieved with AC alone, and images produced by OSEM with both DRC and AC appeared to be qualitatively and quantitatively superior to those produced by OSEM without DRC even if statistical noise exists.

Limitation and future works

Some limitations should be discussed here. In our investigation, an increase of about 6 times in computing time was seen compared with the conventional OSEM algorithm. Almost all the computational effort was expended on the calculation of Gauss function and convolution. Moreover, the optimal iteration number with DRC was larger than that with no compensation and AC only. Hutton et al.[24] also reported that the increase in computation time was about 4 times in the case of subset 2. Despite the long computation time and slow convergence, the DRC algorithm is valuable for clinical application to brain study. We believe this problem can be solved by using a large memory to store the convolution kernel for all projection angles and by improving of the computation performance, so this problem will be minor.

To apply the present method to the fan beam collimator, it cannot be used just as it is. FWHM of the response function is not only dependent on the distance, but also the lateral position of the γ-ray incidence on the detector. That is, the parameter σ, which determines the form with Gauss function, becomes a function of d and x. When measuring this, the present method can be applied to the fan-beam projection data.

In this study we excluded the effect of Compton scatter in the simulation. Scatter correction is generally done when preprocessing reconstruction. The triple energy window (TEW) method[27–29] is well established for scatter compensation with sub-window images. The TEW method uses measurements either below and/or above the photopeak as reference points for the linear interpolation used to estimate the scatter components. A new technique for scatter compensation was recently developed based on the transmission images, namely, a transmission-dependent convolution-subtraction (TDCS) method.[30–32] The estimated scatter component using these methods is subtracted from the projection data. Instead of subtracting the scatter component, one can incorporate scatter compensation as a part of the OSEM algorithm.[12,33–35] In addition, the scatter function can be included directly into the C_{ij} as with the detector response.[33–35] The attenuation, scatter and distance-dependent resolution compensation should be performed for fully quantitative SPECT reconstruction.

CONCLUSION

In this study we demonstrated the effectiveness of 3D distance-dependent resolution compensation with OSEM. We investigated the basic properies of the algorithm by using the point source phantom and applied the digital brain phantom for estimating the accuracy of the cerebral perfusion study. Our results suggested that the implemented OSEM with AC and DRC was reasonably successful for achieving isotropic and stationary resolution and improving contrast in the brain SPECT study.

ACKNOWLEDGMENTS

This research was supported by the "Working group for SPECT reconstruction" in Japanese Society of Radiological Technology. We thank to Messrs. Tomoaki Yamamoto, Seiji Shirakawa, and Tetsuo Kida, who are the member of the working group, for helpful discussion. We also thank to Dr. Yuichiro Narita of Chiba Cancer Center for providing the digital brain phantom, and thank to Dr. Takeyuki Hashimoto of Yokohama Soei College for discussion of simulation. Part of this study was presented at the 57th Annual Meeting of the Japanese Society of Radiological Technology (April 6, 2001, Kobe).

REFERENCES

1. Lewitt RM, Edholm PR, Xia W. Fourier method for correction of depth-dependent collimator blurring. *Proceeding of SPIE* 1989; 1092: 232–243.
2. Zeng GL, Gullberg GT. Frequency domain implementation of the three-dimensional geometric point response correction in SPECT imaging. *IEEE Trans Nucl Sci* 1992; 39: 1444–1453.
3. van Elmbt L, Walrand S. Simultaneous correction of attenuation and distance-dependent resolution in SPECT: an analytical approach. *Phys Med Biol* 1993; 38: 1207–1217.
4. Glick S, Penney B, King M, Byrne CL. Noniterative compensation of photon attenuation and the distance-dependent detector response in SPECT imaging. *IEEE Trans Med Imag* 1994; 13: 363–374.
5. Xia W, Lewitt RM, Edholm PR. Fourier correction for spatially variant collimator blurring in SPECT. *IEEE Trans Med Imag* 1995; 14: 100–115.
6. Liang Z, Ye J, Li CJ, Harrington D. Quantitative cardiac SPECT in three dimensions: validation by experimental phantom studies. *Phys Med Biol* 1998; 43: 905–920.
7. Shinohara H, Yamamoto T, Sugimoto H, Hashimoto T, Takahashi M, Yokoi T. Scatter, attenuation and detector response correction of SPECT. *Med Imag Tech* 2000; 18: 24–32.
8. Ogawa K, Katsu H. Iterative correction method of shift-

variant blurring caused by collimator aperture in SPECT. *Ann Nucl Med* 1996; 10: 33–40.
9. Shepp LA, Vardi Y. Maximum likelihood reconstruction for emission tomography. *IEEE Trans Med Imag* 1982; 1: 113–122.
10. Hudson HM, Larkin RS. Accelerated image reconstruction using ordered subsets of projection data. *IEEE Trans Med Imag* 1994; 13: 601–609.
11. Murase K, Tanada S, Inoue T, Sugawara Y, Hamamoto K. Improvement of brain SPET using transmission data acquisition in a four-head SPET scanner. *Eur J Nucl Med* 1993; 20: 32–38.
12. Matsuoka S, Shinohara H, Yamamoto S, Niio Y, Shima H, Yamada M, et al. Combined scatter and attenuation correction for Tl-201 myocardial perfusion SPECT using OS-EM algorithm. *Nippon Acta Radiologica* 1998; 58: 751–757.
13. Tsui BMW, Hu HB, Gilland DR, Gullberg GT. Implementation of simultaneous attenuation and detector response correction in SPECT. *IEEE Trans Nucl Sci* 1988; 35: 778–783.
14. Formiconi AR, Pupi A, Passeri A. Compensation of spatial system response in SPECT with conjugate gradient reconstruction technique. *Phys Med Biol* 1989; 34: 69–84.
15. Zeng GL, Gullberg GT, Tsui BMW, Terry JA. Three-dimensional iterative reconstruction algorithms with attenuation and geometric point response correction. *IEEE Trans Nucl Sci* 1991; 38: 693–702.
16. Liang Z, Turkington TG, Gilland DR, Jaszczak RJ, Coleman RE. Simultaneous compensation for attenuation, scatter and detector response for SPECT reconstruction in three dimensions. *Phys Med Biol* 1992; 37: 587–603.
17. Tsui BMW, Zhao X, Frey EC, Gullberg GT. Comparison between ML-EM and WLS-CG algorithms for SPECT image reconstruction. *IEEE Trans Med Imag* 1994; 13: 601–609.
18. Ju Z-W, Frey EC, Tsui BMW. Distributed 3-D iterative reconstruction for quantitative SPECT. *IEEE Trans Nucl Sci* 1995; 42: 1301–1309.
19. Pan T-S, Luo D-S, Kohli V, King MA. Influence of OSEM, elliptical orbits and background activity on SPECT 3D resolution recovery. *Phys Med Biol* 1997; 42: 2517–2529.
20. Pretorius PH, King MA, Pan T-S, de Vries DJ, Glick SJ, Byrne CL. Reducing the influence of the partial volume effect on SPECT activity quantitation with 3D modeling of spatial resolution in iterative reconstruction. *Phys Med Biol* 1998; 43: 407–420.
21. Kohli V, King MA, Glick SJ, Pan TS. Comparison of frequency-distance relationship and Gaussian-diffusion-based method of compensation for distance-dependent spatial resolution in SPECT imaging. *Phys Med Biol* 1998; 43: 1025–1037.
22. Fleming JS, Simpson DE. A technique for simulation of the point spread function of a gamma camera. *Phys Med Biol* 1994; 39: 1457–1473.
23. Kao C-M, Pan X. Non-iterative methods incorporating a priori source distribution and data information for suppression of image noise and artifacts in 3D SPECT. *Phys Med Biol* 2000; 45: 2801–2819.
24. Hutton BF, Lau YH. Application of distance-dependent resolution compensation and post-reconstruction filtering for myocardial SPECT. *Phys Med Biol* 1998; 43: 1679–1693.
25. Salamon G, Huang YP. *Computed Tomography of the Brain*. Berlin-Heidelberg-New York; Springer-Verlag, 1980.
26. Yokoi T, Shinohara H, Hashimoto T, Yamamoto T, Niio Y. Implementation and performance evaluation of iterative reconstruction algorithms in SPECT: a simulation study using EGS4. Proceeding of the Second International Workshop on EGS. *KEK Proceedings* 2000; 20: 224–234.
27. Ogawa K, Harata Y, Ichihara T, Kubo A, Hashimoto S. A practical method for position-dependent Compton-scatter correction in single-photon emission CT. *IEEE Trans Med Imag* 1991; 10: 408–412.
28. Ichihara T, Ogawa K, Motomura N, Kubo A, Hashimoto S. Compton scatter compensation using the triple-energy window method for single- and dual-isotope SPECT. *J Nucl Med* 1993; 34: 2216–2221.
29. Hashimoto J, Ogawa K, Kubo A, Ichihara T, Motomura N, Takayama T, et al. Application of transmission scan-based attenuation compensation to scatter-corrected thallium-201 myocardial single-photon emission tomographic images. *Eur J Nucl Med* 1998; 25: 120–127.
30. Meikle SR, Hutton BF, Bailey DL. A transmission dependent method for scatter correction in SPECT. *J Nucl Med* 1994; 35: 360–367.
31. Narita Y, Eberl S, Iida H, Hutton BF, Braun F, Nakamura T, et al. Monte Carlo and experimental evaluation of accuracy and noise properties of two scatter correction methods for SPECT. *Phys Med Biol* 1996; 41: 2481–2496.
32. Iida H, Narita Y, Kado H, Kashikura A, Sugawara S, Shoji Y, et al. Effects of scatter and attenuation correction on quantitative assessment of regional cerebral blood flow with SPECT. *J Nucl Med* 1998; 39: 181–189.
33. Welch A, Gullberg G. Implementation of a model-based nonuniform scatter correction scheme for SPECT. *IEEE Trans Med Imag* 1997; MI-16: 717–726.
34. Beekman FJ, Kamphuis C, Frey EC. Scatter compensation methods in 3D iterative SPECT reconstruction: a simulation study. *Phys Med Biol* 1997; 42: 1619–1632.
35. Beekman FJ, den Harder JM, Viergever MA, van Rijk PP. SPECT scatter modeling in non-uniform attenuating objects. *Phys Med Biol* 1997; 42: 1133–1142.
36. Press WH, Teukolsky SA, Vetterling WT, Flannery BP. *1993 Numerical Recipes in C.* Japanese Edition (Tokyo; Gijutsu Hyoron Sha).
37. Yokoi T. Implementation of reconstruction program using maximum likelihood-expectation maximization (ML-EM) algorithm. *Jpn J Nucl Med Tech [Kaku-Igaku gijutsu]* 2000; 20: 331–340.
38. Maniawski PJ, Morgan HT, Wackers FJT. Orbit-related variation in spatial resolution as a source of artifactual defects in thallium-201 SPECT. *J Nucl Med* 1991; 32: 871–875.